Chapter 6

Heat Transfer of Supercritical Fluid Flows and Compressible Flows

Yu Ito

Additional information is available at the end of the chapter

http://dx.doi.org/10.5772/65931

Abstract

In this chapter, the heat transfer between supercritical fluid flows and solid walls and that between compressible flows and solid walls is described. First, the physical fundamentals of supercritical fluids and compressible flows are explained. Second, methods for estimating the heat-transfer performance according to the physical fundamentals and conventional experimental results are described. Then, the known correlations for estimating the heat-transfer performance are introduced. Finally, examples of practical heat exchangers using supercritical fluid flows and/or compressible flows are presented.

Keywords: supercritical fluid flow, compressible flow, nusselt number, reynolds number, mach number, pressure coefficient distribution

1. Introduction

The range of use of heat exchangers is being expanded to extensive applications in various fields. In particular, supercritical fluids and high-speed air, that is,, compressible fluids, are suitable as working fluids.

Supercritical fluid is a phase of substances, in addition to the solid, liquid, and gas phases. In particular, in the vicinity of the critical point, many physical properties behave in an unusual way. For example, the density, viscosity, and thermal conductivity drastically change at the critical point, the specific heat and thermal expansion ratios diverge at the critical point, and the sound velocity is zero at the critical point. The physical properties of a supercritical fluid must be evaluated by the appropriate equation of state and equation of the transport properties.

On the other hand, a compressible flow can be assumed as an ideal gas, but additional dynamic energy, that is, the Mach-number effect, must be considered. Therefore, three types

of pressures (static, total, and dynamic), four types of temperatures (static, total, dynamic, and recovery), the difference between laminar and turbulent boundary layers, etc., should be distinguished and treated.

2. Equations of state and transport properties of supercritical fluid

Figure 1 shows the *P*–*T* diagram of a pure substance (water in this case), which is also called a phase diagram. The sublimation curve divides the solid and gas phases, the melting curve divides the solid and liquid phases, and the vaporization curve divides the liquid and gas phases. Two phases coexist on these three curves. When the pressure and/or temperature change across these three coexistence curves of solid-gas, solid-liquid, and liquid-gas, the density discontinuously changes. These three coexistence curves meet at the triple point, which is the unique point where solid, liquid, and gas coexist in equilibrium.

The vaporization curve ends at the critical point. On the vaporization curve, liquid is called the saturation liquid, and gas is called the saturation gas (vapor). When approaching the critical point along the vaporization curve, the density of the saturation liquid decreases, and the density of the saturation gas (vapor) increases. Finally, they meet at the critical point. Fluid overtaking the critical point in temperature and pressure is called the "supercritical fluid."

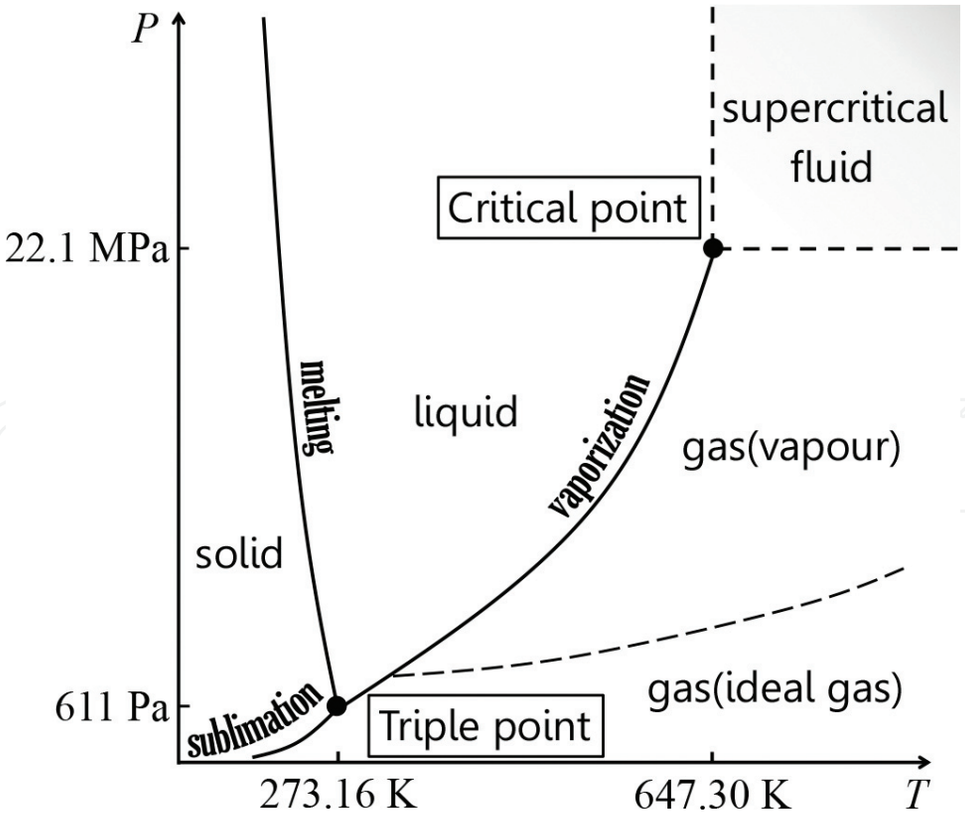

Figure 1. Phase chart on P-T diagram (for water).

Solid	Diffusivity << condensability
Liquid	Diffusivity < condensability
Supercritical fluid	Diffusivity ≈ condensability
Gas (vapor)	Diffusivity > condensability
Gas (ideal gas)	Diffusivity >> condensability

The phase is thermodynamically determined by the Gibbs free energy G:

$$G = H - TS = U - TS + PV \tag{1}$$

Where H is the enthalpy, S is the entropy, U is the internal energy, and V is the specific volume [1].

That is, the phase is determined by the balance between the diffusivity caused by the thermal mobility of the molecules and the condensability by intermolecular forces. The diffusivity caused by thermal mobility increases with the temperature. The condensability by intermolecular forces increases with the density. In general, the following relationships hold:

In **Figure 1**, the first-order differentials of the Gibbs free energy

$$dG = -SdT + VdP \tag{2}$$

$$\left(\frac{dG}{dT}\right)_{\mathrm{P}} = -S \tag{3}$$

$$\left(\frac{dG}{dP}\right)_{\mathrm{T}} = V = \frac{1}{\rho} \tag{4}$$

are discontinuous across the three coexistence curves, but the first-order differentials of the Gibbs free energy are continuous at the critical point. In addition, the second-order differentials of the Gibbs free energy are discontinuous at the critical point.

$$\left(\frac{d^2G}{dT^2}\right)_{\mathrm{P}} = -\frac{1}{T}\left(\frac{dH}{dT}\right)_{\mathrm{P}} = -\frac{1}{T}C_{\mathrm{P}} \tag{5}$$

$$\left(\frac{d^2G}{dP^2}\right)_{\mathrm{T}} = \left(\frac{dV}{dP}\right)_{\mathrm{T}} = -VK_{\mathrm{T}} \tag{6}$$

Here, ρ is the density, C_{P} is the isobaric specific heat, and K_{T} is the isothermal compressibility. At the critical point, the density drastically changes, the specific heat and thermal expansion ratio diverge, and the sound velocity is zero.

Figures 2 and **3** show the isobaric and isothermal changes of the density, viscosity, and kinematic viscosity by using the data from references [2, 3]. Both the density (derived from

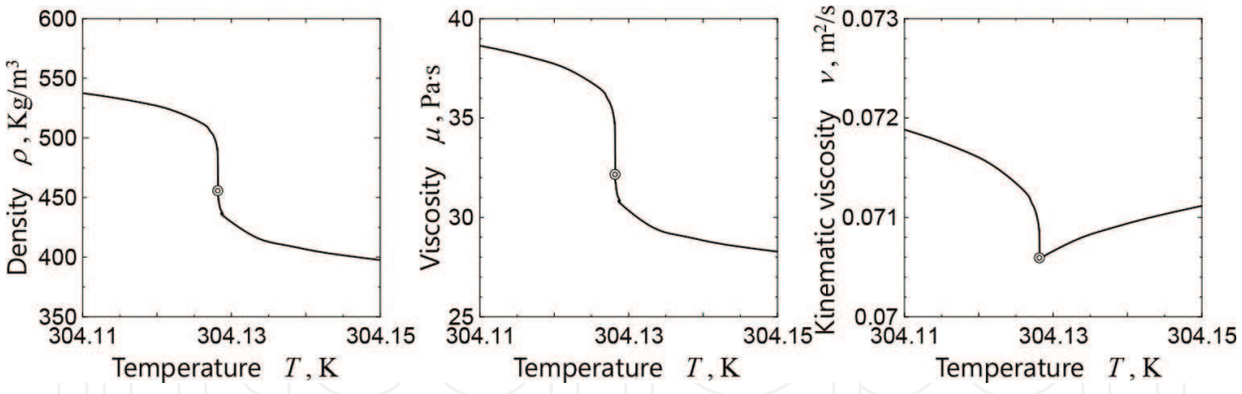

Figure 2. Isobaric changes of the density, viscosity, and kinematic viscosity near the critical point where $T_{critical}$ = 304.1282 K and $P_{critical}$ = 7.3773 MPa (for carbon dioxide).

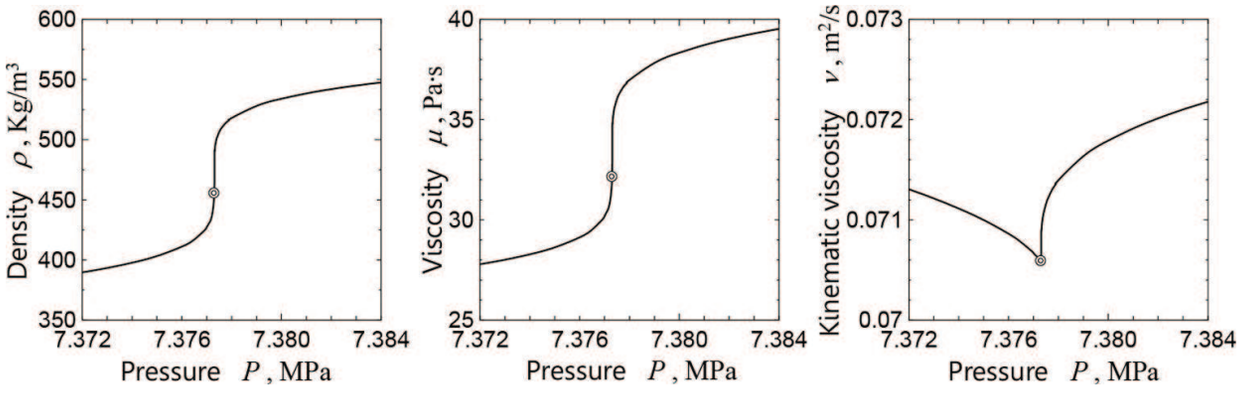

Figure 3. Isothermal changes of the density, viscosity, and kinematic viscosity near the critical point where $T_{critical}$ = 304.1282 K and $P_{critical}$ = 7.3773 MPa (for carbon dioxide).

the equation of state) and the viscosity (derived from the equation of the transport properties) drastically change at the critical point, and the derivatives with respect to temperature and pressure diverge at the critical point. The kinematic viscosity (combined with the density and viscosity) has an extremum value at the critical point. The equations of state and the transport properties should consider these types of tricky features in the vicinity of the critical point for transcritical- and supercritical-fluid flows.

The most important substances in practical applications are carbon dioxide and water, although all substances have a supercritical-fluid phase. Recently, accurate correlations for the equations of state and the transport properties containing the critical point have been proposed.

For carbon dioxide, Span and Wagner proposed the equation of state from the triple point to 1100 K at pressures up to 800 MPa [2]. Their equation of state is briefly introduced here. They expressed the fundamental equation in the form of the Helmholtz energy A:

$$A = U - TS = H - RT - TS \tag{7}$$

with two independent variables—the density ρ and temperature T. The dimensionless Helmholtz energy $\phi = A/RT$ is divided into a part obeying the ideal gas behavior ϕ° and a part that deviates from the ideal gas behavior ϕ^{r} [2]:

$$\phi(\delta,\tau) = \phi^{\circ}(\delta,\tau) + \phi^{\mathrm{r}}(\delta,\tau), \tag{8}$$

Where $\delta = \rho/\rho_{\mathrm{c}}$ is the reduced density; $\tau = T_{\mathrm{c}}/T$ is the inverse reduced temperature; and ρ_{c} and T_{c} are the density and temperature, respectively, at the critical point. Then, all of the other thermodynamic properties can be obtained by the combined derivatives of Eq. (7) using the Maxwell relations [1].

Pressure

$$P(T,\rho) = -\left(\frac{\partial A}{\partial V}\right)_{\mathrm{T}} \text{then} \frac{P(\delta,\tau)}{\rho RT} = 1 + \delta\phi^{\mathrm{r}}_{\delta} \tag{9}$$

Entropy

$$S(T,\rho) = -\left(\frac{\partial A}{\partial T}\right)_{\mathrm{V}} \text{then} \frac{S(\delta,\tau)}{R} = \tau[\phi^{\circ}_{\tau} + \phi^{\mathrm{r}}_{\tau}] - \phi^{\circ} - \phi^{\mathrm{r}} \tag{10}$$

Internal energy

$$U(T,\rho) = A - T\left(\frac{\partial A}{\partial T}\right)_{\mathrm{V}} \text{then} \frac{U(\delta,\tau)}{RT} = \tau[\phi^{\circ}_{\tau} + \phi^{\mathrm{r}}_{\tau}] \tag{11}$$

Isochoric specific heat

$$C_{\mathrm{V}}(T,\rho) = \left(\frac{\partial U}{\partial T}\right)_{\mathrm{V}} \text{then} \frac{C_{\mathrm{V}}(\delta,\tau)}{R} = -\tau^2[\phi^{\circ}_{\tau\tau} + \phi^{\mathrm{r}}_{\tau\tau}] \tag{12}$$

Enthalpy

$$H(T,\rho) = A - T\left(\frac{\partial A}{\partial T}\right)_{\mathrm{V}} - V\left(\frac{\partial A}{\partial V}\right)_{\mathrm{T}} \text{then} \frac{H(\delta,\tau)}{RT} = 1 + \tau[\phi^{\circ}_{\tau} + \phi^{\mathrm{r}}_{\tau}] + \delta\phi^{\mathrm{r}}_{\delta} \tag{13}$$

Isobaric specific heat

$$C_{\mathrm{P}}(T,\rho) = \left(\frac{\partial H}{\partial T}\right)_{\mathrm{P}} \text{then} \frac{C_{\mathrm{P}}(\delta,\tau)}{R} = -\tau^2[\phi^{\circ}_{\tau\tau} + \phi^{\mathrm{r}}_{\tau\tau}] + \frac{[1 + \delta\phi^{\mathrm{r}}_{\delta} - \delta\tau\phi^{\mathrm{r}}_{\delta\tau}]^2}{1 + 2\delta\phi^{\mathrm{r}}_{\delta} + \delta^2\phi^{\mathrm{r}}_{\delta\delta}} \tag{14}$$

Saturated specific heat

$$C_{\sigma}(T) = \left(\frac{\partial H}{\partial T}\right)_{\mathrm{P}} + T\left(\frac{\partial P}{\partial T}\right)_{\mathrm{V}}\left(\frac{\partial P_{\mathrm{sat}}}{\partial T}\right) \Big/ \left(\frac{\partial P}{\partial V}\right)_{\mathrm{T_{sat}}} \tag{15}$$

then,

$$\frac{C_{\sigma}(\delta,\tau)}{R} = -\tau^2[\phi^{\circ}_{\tau\tau} + \phi^{\mathrm{r}}_{\tau\tau}] + \frac{1 + \delta\phi^{\mathrm{r}}_{\delta} - \delta\tau\phi^{\mathrm{r}}_{\delta\tau}}{1 + 2\delta\phi^{\mathrm{r}}_{\delta} + \delta^2\phi^{\mathrm{r}}_{\delta\delta}}\left[\{1 + \delta\phi^{\mathrm{r}}_{\delta} - \delta\tau\phi^{\mathrm{r}}_{\delta\tau}\} - \frac{\rho_{\mathrm{c}}}{R\delta}\frac{dP_{\mathrm{sat}}}{dT}\right] \tag{16}$$

Speed of sound

$$w(T,\rho)=\sqrt{\left(\frac{\partial P}{\partial \rho}\right)_{\mathrm{S}}}\ \text{then}\ \frac{w^2(\delta,\tau)}{RT}=1+2\delta\phi_{\delta}^{\mathrm{r}}+\delta^2\phi_{\delta\delta}^{\mathrm{r}}-\frac{[1+\delta\phi_{\delta}^{\mathrm{r}}-\delta\tau\phi_{\delta\tau}^{\mathrm{r}}]^2}{\tau^2[\phi_{\tau\tau}^{\circ}+\phi_{\tau\tau}^{\mathrm{r}}]} \tag{17}$$

etc.

Here,

$$\phi_{\delta}=\left(\frac{\partial\phi}{\partial\delta}\right)_{\tau},\ \phi_{\delta\delta}=\left(\frac{\partial^2\phi}{\partial\delta^2}\right)_{\tau},\ \phi_{\tau}=\left(\frac{\partial\phi}{\partial\tau}\right)_{\delta},\ \phi_{\tau\tau}=\left(\frac{\partial^2\phi}{\partial\tau^2}\right)_{\delta}\ \text{and}\ \phi_{\delta\tau}=\left(\frac{\partial^2\phi}{\partial\delta\partial\tau}\right).$$

For carbon dioxide, Vesovic et al. proposed transport properties in the temperature range of 200–1500 K for the viscosity μ and in the temperature range of 200–1000 K for the thermal conductivity k [3]. Their equations of the transport properties μ and k are briefly introduced. Their fundamental equation combines three independent parts: a part obeying the ideal gas behavior $\mu^{\circ}(T)$ and $k^{\circ}(T)$, a part with excess properties because of the elevated density $\Delta\mu(\rho,T)$ and $\Delta k(\rho,T)$, and a part with an enhancement in the vicinity of the critical point $\Delta_{\mathrm{c}}\mu(T)$ and $\Delta_{\mathrm{c}}k(T)$:

$$\mu(\rho,T)=\mu^{\circ}(T)+\Delta\mu(\rho,T)+\Delta_{\mathrm{c}}\mu(T) \tag{18}$$

$$k(\rho,T)=k^{\circ}(T)+\Delta k(\rho,T)+\Delta_{\mathrm{c}}k(T) \tag{19}$$

For water, Wagner and Pruß proposed the equation of state for the temperature range of 251.2–1273 K and pressures up to 1000 MPa [4]. Huber et al. proposed the transport properties from the melting temperature to 1173 K at 1000 MPa [5, 6].

3. Heat transfers between supercritical fluid flow and solid

As mentioned in Section 2, the kinematic viscosity of a supercritical fluid is less than those of a liquid and gas; therefore, the Reynolds number, Re, of a supercritical fluid flow is higher than those of a liquid and gas flow with the same velocity, and a turbulent flow is easily formed. For heat transfer in a turbulent flow, Dittus and Boelter proposed a correlation of the Nusselt number using the Re and Prandtl number, Pr, for a liquid flow in a circular automobile radiator [7] as shown in **Figure 4**.

$$\mathrm{Nu}_{\mathrm{local,\,turb}}=0.023\mathrm{Re}_{\mathrm{local}}^{0.8}\mathrm{Pr}_{\mathrm{local}}^{n} \tag{20}$$

$$\mathrm{Re}_{\mathrm{local}}=\frac{u_{\mathrm{local}}D}{\nu_{\mathrm{local}}}=\frac{\rho_{\mathrm{local}}u_{\mathrm{local}}D}{\mu_{\mathrm{local}}}=\frac{4m}{\pi D\mu_{\mathrm{local}}} \tag{21}$$

$$\mathrm{Pr}_{\mathrm{local}}=\frac{\nu_{\mathrm{local}}}{\kappa_{\mathrm{local}}}=\frac{\mu_{\mathrm{local}}C_{\mathrm{P,local}}}{k_{\mathrm{local}}} \tag{22}$$

Here, the superscript $n=0.3$ for $T_{\mathrm{wall}}<T_{\mathrm{fluid}}$ or $n=0.4$ for $T_{\mathrm{wall}}>T_{\mathrm{fluid}}$, u_{local} is the average velocity across the cross section, D is the diameter of the tube, μ is the viscosity, m is the mass

http://dx.doi.org/10.5772/65931

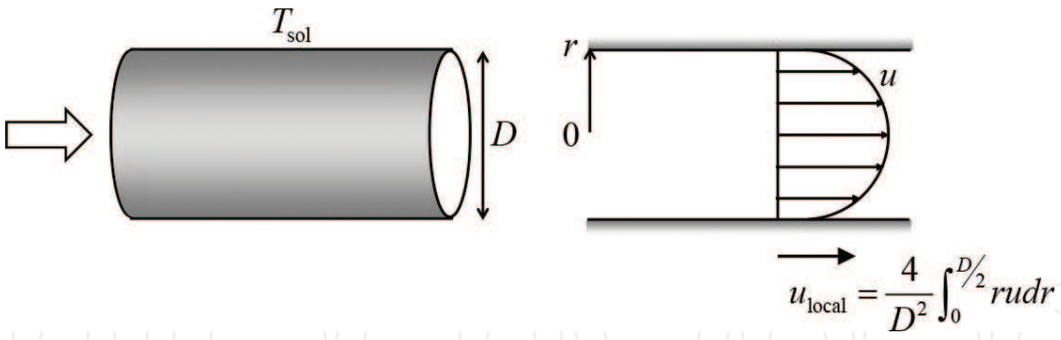

Figure 4. Heat transfer between a supercritical fluid flow and a circular solid tube wall.

flow rate, κ is the thermal diffusivity, and k is the heat conductivity. For liquid and gas flows, the fluid properties and flow conditions can be regarded as constant throughout the entire region in most practical cases because the fluid properties are insensitive to temperature and pressure changes in the tube. Therefore, the inlet values of the physical properties and flow conditions can be used, and Re and Pr can be regarded as constant throughout the entire tube. On the other hand, the fluid properties of a supercritical fluid are very sensitive to temperature and pressure changes in the tube. Thus, in the tube, the density gradually changes because of the heat input and/or pressure loss, the local average velocity changes, and even Re and Pr change. Unfortunately, the Dittus-Boelter correlation with the inlet values of the physical properties and flow conditions cannot be directly used for heat transfer in a supercritical turbulent flow. Liao and Zhao measured the rate of the heat transfer between a supercritical carbon dioxide flow and a circular solid tube wall for $T_{wall} < T_{fluid}$ [8]. Their tube was set in the horizontal direction. They proposed a correlation of area-averaged Nusselt numbers as functions of the Reynolds and Prandtl numbers defined at the temperatures of the mean bulk and the wall.

$$\mathrm{Nu}_{\mathrm{ave,turb}} = 0.128\mathrm{Re}_{\mathrm{wall}}^{0.8}\mathrm{Pr}_{\mathrm{wall}}^{0.3}\left[\frac{\mathrm{Gr}}{\mathrm{Re}_{\mathrm{bulk}}^2}\right]^{0.205}\left[\frac{\rho_{\mathrm{bulk}}}{\rho_{\mathrm{wall}}}\right]^{0.437}\left[\frac{\mathrm{C}_{\mathrm{P,bulk}}}{\mathrm{C}_{\mathrm{P,wall}}}\right]^{0.411}\ \mathrm{for}\mathrm{CO}_2 \tag{23}$$

$$\mathrm{Gr} = \frac{[\rho_{\mathrm{wall}} - \rho_{\mathrm{bulk}}]\rho_{\mathrm{bulk}} g D^3}{\mu_{\mathrm{bulk}}^2} \tag{24}$$

$$\mathrm{Re}_{\mathrm{bulk}} = \frac{4m}{\pi D\mu(T_{\mathrm{bulk}}, P_{\mathrm{bulk}})} \tag{25}$$

$$\rho_{\mathrm{bulk}} = \rho(T_{\mathrm{bulk}}, P_{\mathrm{bulk}}) \tag{26}$$

$$\mu_{\mathrm{bulk}} = \mu(T_{\mathrm{bulk}}, P_{\mathrm{bulk}}) \tag{27}$$

$$\mathrm{Re}_{\mathrm{wall}} = \frac{4m}{\pi D\mu(T_{\mathrm{wall}}, P_{\mathrm{wall}})} \tag{28}$$

$$\mathrm{Pr}_{\mathrm{wall}} = \frac{\nu(T_{\mathrm{wall}}, P_{\mathrm{wall}})}{\kappa(T_{\mathrm{wall}}, P_{\mathrm{wall}})} = \frac{\mu(T_{\mathrm{wall}}, P_{\mathrm{wall}})C_{\mathrm{P}}(T_{\mathrm{wall}}, P_{\mathrm{wall}})}{k(T_{\mathrm{wall}}, P_{\mathrm{wall}})} \tag{29}$$

$$\rho_{\text{wall}} = \rho(T_{\text{wall}}, P_{\text{wall}}) \tag{30}$$

$$C_{\text{P,wall}} = C_{\text{P}}(T_{\text{wall}}, P_{\text{wall}}) \tag{31}$$

$$C_{\text{P,bulk}} = C_{\text{P}}(T_{\text{bulk}}, P_{\text{bulk}}) \tag{32}$$

Here, $T_{\text{bulk}} = [T_{\text{in}} + T_{\text{out}}]/2$ and T_{wall} are constant. This correlation is applicable in the range of 7.4 MPa $< P_{\text{bulk}} <$ 12.0 MPa, 20°C $< T_{\text{bulk}} <$ 110°C, 2°C $< T_{\text{bulk}} - T_{\text{wall}} <$ 30°C, 0.02 kg/min $< \dot{m} <$ 0.2 kg/min, $1025 < \text{Gr}/\text{Re}_{\text{bulk}}^2 < 1022$ for the horizontal long tubes of 0.50 mm $< d <$ 2.16 mm.$\text{Re}_{\text{wall}}^{0.8}$ and $\text{Pr}_{\text{wall}}^{0.3}$ were originally derived from the Dittus-Boelter correlation. $\text{Gr}/\text{Re}_{\text{bulk}}^2$ is the effect of buoyancy in the radial direction of a horizontal tube. The density of fluid at a temperature and pressure in the vicinity of the critical point is very sensitive to changes in temperature; thus, the effect of the buoyancy derived from the temperature difference between the bulk and wall cannot be ignored. This effect is enhanced as the diameter of the tube increases.

Ito et al. proposed an airfoil heat exchanger, which is applied between a compressible airflow and a liquid or a supercritical fluid flow [9]. It has an outer airfoil shape suitable for high-speed airflow and contains several tubes for a high-pressure liquid or a supercritical fluid flow. The researchers installed a cascade of airfoil heat exchangers into a subsonic wind tunnel at a temperature of T_{air} and measured the heat-transfer coefficient of a liquid or a supercritical fluid flow at a temperature of $T_{\text{scf}} < T_{\text{air}}$ in a vertical tube. They derived correlations for supercritical carbon dioxide and compressed water at a pressure of $P_{\text{scf}} \leq 30$ MPa as follows:

$$\text{Nu}_{\text{ave,turb}} = \begin{cases} 0.0230\text{Re}^{0.808}\text{Pr}^{0.300} & \text{for} H_2O \\ 0.0231\text{Re}^{0.823}\text{Pr}^{0.300} & \text{for} CO_2 \end{cases} \tag{33}$$

These correlations are very simple and similar to the Dittus-Boelter correlation in Eq. (20) but have sufficient accuracy. Ito et al. used accurate equations of state and the transport properties, as mentioned in Section 2. They said in reference [9] that ordinary correlations (of course, containing the Dittus-Boelter correlation) for liquid and gas can be used when sufficiently accurate equations of state and the transport properties are used. However, the physical properties at a temperature and pressure in the vicinity of the critical point continuously change throughout the tube because of the heat input and/or pressure loss; therefore, changes in these physical properties throughout the tube should be sufficiently considered. For example, the present author recommends the numerical integration of local heat transfer correlations using local accurate physical properties for the entire tube.

4. Thermofluid dynamics of compressible flow on solid wall

4.1. Meanings of temperature and pressure of compressible flow

A stationary fluid pressure of P [Pa], specific volume of V [m^3/kg], and constant temperature T stores a mechanical energy of e_{pre} [J/kg]. Here,

$$e_{\mathrm{pre}} = PV. \tag{34}$$

The "pressure" (often called "static pressure") P is the potential of the mechanical energy level contained in a stationary fluid. A motional fluid has an additional dynamic energy e_{dyn} [J/kg]:

$$e_{\mathrm{dyn}} = \frac{1}{2}u^2. \tag{35}$$

in addition to e_{pre}; therefore,

$$e_{\mathrm{pre}} + e_{\mathrm{dyn}} = PV + \frac{1}{2}u^2 = V[P + P_{\mathrm{dyn}}] = VP_{\mathrm{tot}} = e_{\mathrm{mech}}. \tag{36}$$

$$P_{\mathrm{dyn}} = \frac{1}{2V}u^2 = \frac{1}{2}\rho u^2. \tag{37}$$

$$P_{\mathrm{tot}} = P + P_{\mathrm{dyn}}. \tag{38}$$

Here, P_{dyn} [Pa] is called "dynamic pressure" and is an index of the dynamic mechanical energy level contained in a motional fluid. Further, e_{mech} [J/kg] is called "total mechanical energy." Moreover, P_{tot} [Pa] is called the "total pressure" and is an index of the total mechanical energy level contained in a motional fluid. Some processes are reversible between mechanical energies of e_{pre} and e_{dyn} in cases where e_{pre} and e_{dyn} transform in the equilibrium processes. For example, using a nozzle, P_{dyn} increases, P decreases, and P_{tot} is constant in an acceleration section, and P_{dyn} decreases, P increases, and P_{tot} is constant in a deceleration section. Some process are irreversible between e_{pre} and e_{dyn} in cases where e_{pre} and e_{dyn} transform in nonequilibrium processes. For example, because of friction, P remains constant, P_{dyn} decreases, and P_{tot} also decreases.

Next, we consider thermal energy. A stationary fluid at an isochoric specific heat of C_{V} [J/(kg K)] stores a relative internal energy of e [J/kg] from e_0 at the standard temperature T_0:

$$e - e_0 = \int_{T_0}^{T} C_{\mathrm{V}} dT. \tag{39}$$

Here, the internal energy is an index of the thermal energy level contained in a stationary fluid. In the case of a constant C_{V},

$$e - e_0 = C_{\mathrm{V}}[T - T_0]. \tag{40}$$

The "temperature" (often called "static temperature") T is an index of the energy level contained in a stationary fluid.

In cases where a fluid is assumed as an ideal gas,

$$PV = RT \Leftrightarrow P = \rho RT, \tag{41}$$

where R is the gas constant, and ρ is the density, which is equal to $1/V$. Then,

$$R = \frac{Pv}{T} = \frac{P_0 v_0}{T_0} \tag{42}$$

A stationary fluid at an isochoric specific heat of C_V [J/(kg K)] stores a relative enthalpy of h [J/kg] from h_0 at the standard temperature of T_0, a pressure of P_0, and a specific volume of V_0. Videlicet, enthalpy is a combination of internal energy and mechanical energy. Here,

$$h–h_0 = [e + PV]–[e_0 + P_0 V_0] = \int_{T_0}^{T} C_V dT + \int_{T_0}^{T} R dT. \tag{43}$$

In the case of a constant C_V,

$$h–h_0 = C_V[T–T_0] + R[T–T_0] = C_P[T–T_0], \tag{44}$$

$$C_P = C_V + R, \tag{45}$$

where C_P is the isobaric specific heat. A motional fluid has an additional dynamic energy e_{dyn} [J/kg], as shown in Eq. (35). If a motional fluid suddenly stops, dynamic energy can be converted into enthalpy. Then, the following equation applies:

$$h–h_0 + e_{dyn} = C_P[T–T_0] + \frac{1}{2}u^2 = C_P[T + T_{dyn}–T_0] = C_P[T_{tot}–T_0]. \tag{46}$$

$$T_{dyn} = \frac{1}{2C_P}u^2. \tag{47}$$

$$T_{tot} = T + T_{dyn}. \tag{48}$$

Here, T_{dyn} [K] is called the "dynamic temperature" and is an index of the dynamic energy level contained in a motional fluid. Moreover, T_{tot} [K] is called the "total temperature" and is an index of the total energy level contained in a motional fluid. Some processes are reversible between mechanical energies of h and e_{dyn} in cases where e_{dyn} transforms into PV in equilibrium processes. For example, using a nozzle, in an acceleration section, T_{dyn} increases, h decreases, T_{tot} is constant, and vice versa. Some processes are irreversible in cases where e_{dyn} transforms into $C_V T$ in nonequilibrium processes. For example, because of friction, T_{dyn} decreases, T increases, and T_{tot} remains constant; however, T cannot be converted into T_{dyn} again.

4.2. Isentropic change and sound speed of ideal gas

The specific heat ratio γ is defined as:

$$\gamma = \frac{C_P}{C_V} \tag{49}$$

From Eqs. (45) and (49),

$$C_V = \frac{R}{\gamma - 1},\ C_P = \frac{\gamma R}{\gamma - 1} \tag{50}$$

This equation is substituted into Eqs. (40) and (44). Then,

$$e - e_0 = \frac{R}{\gamma - 1}[T - T_0],\quad h - h_0 = \frac{\gamma R}{\gamma - 1}[T - T_0] \tag{51}$$

$$de = \frac{R}{\gamma - 1}dT, dh = \frac{\gamma R}{\gamma - 1}dT \tag{52}$$

The change in the entropy ds is defined as:

$$Tds = de + pdV, Tds = dh - VdP \tag{53}$$

$$ds = \frac{de + pdV}{T}, ds = \frac{dh - VdP}{T} \tag{54}$$

When isentropic change $ds = 0$,

$$0 = ds = C_V\frac{dT}{T} + R\frac{dV}{V}, 0 = ds = C_P\frac{dT}{T} - R\frac{dP}{P} \tag{55}$$

$$0 = \frac{R}{\gamma - 1}\frac{dT}{T} - R\frac{d\rho}{\rho}, 0 = \frac{\gamma R}{\gamma - 1}\frac{dT}{T} - R\frac{dP}{P} \tag{56}$$

$$\frac{1}{\gamma - 1}\frac{dT}{T} = \frac{d\rho}{\rho},\ \frac{\gamma}{\gamma - 1}\frac{dT}{T} = \frac{dP}{P} \tag{57}$$

We totally differentiate Eq. (41), obtaining the following:

$$dP = RTd\rho + \rho TdR + \rho RdT \tag{58}$$

$$\frac{dP}{P} = \frac{d\rho}{\rho} + \frac{dR}{R} + \frac{dT}{T} = \frac{d\rho}{\rho} + \frac{dT}{T} \Leftrightarrow \frac{dT}{T} = \frac{dP}{P} - \frac{d\rho}{\rho} \tag{59}$$

We substitute the final equation of Eq. (59) and Eq. (45) into the rightmost part of Eq. (55):

$$0 = ds = C_P \frac{dT}{T} - R\frac{dP}{P} = C_P \frac{dP}{P} - C_P \frac{d\rho}{\rho} - R\frac{dP}{P} = C_V \frac{dP}{P} - C_P \frac{d\rho}{\rho} \tag{60}$$

$$0 = \frac{R}{\gamma - 1}\frac{dP}{P} - \frac{\gamma R}{\gamma - 1}\frac{d\rho}{\rho} \tag{61}$$

$$\gamma \frac{d\rho}{\rho} = \frac{dP}{P} \tag{62}$$

$$\frac{dP}{d\rho} = \gamma \frac{P}{\rho} \tag{63}$$

We integrate Eqs. (57) and (62):

$$\frac{T}{\rho^{\gamma-1}} = \text{const}, \quad \frac{T}{P^{\frac{\gamma-1}{\gamma}}} = \text{const}, \quad \frac{P}{\rho^{\gamma}} = \text{const} \tag{64}$$

The sound speed a is defined as:

$$a^2 = \left[\frac{dP}{d\rho}\right]_S \tag{65}$$

Eqs. (63) and (41) are substituted into Eq. (65), yielding the following:

$$a^2 = \gamma \frac{P}{\rho} = \gamma RT \tag{66}$$

4.3. Relationships of static and total values in isentropic compressible flow

The one-dimensional energy equation of an isentropic flow at an arbitrary cross section is derived by using Eq. (46) as:

$$h + \frac{1}{2}u^2 = \text{const} \tag{67}$$

When the enthalpy and velocity are h_1 and u_1 at an arbitrary cross section 1,

$$h_1 + \frac{1}{2}u_1^2 = h + \frac{1}{2}u^2 \tag{68}$$

This relationship is true even if cross section 1 corresponds to the stagnant cross section 0 (h_0 and $u_0 = 0$); therefore,

$$h_0 = h + \frac{1}{2}u^2 \tag{69}$$

Eqs. (44) and (50) are substituted into Eq. (69), yielding the following:

$$\frac{\gamma RT_0}{\gamma-1} = \frac{\gamma RT}{\gamma-1} + \frac{1}{2}u^2 \tag{70}$$

Eq. (66) is substituted into Eq. (70):

$$\frac{a_0^2}{\gamma-1} = \frac{a^2}{\gamma-1} + \frac{1}{2}u^2 \tag{71}$$

We multiply by $\frac{\gamma-1}{a^2}$ and substitute Eq. (66), obtaining the following:

$$\frac{a_0^2}{a^2} = \frac{RT_0}{RT} = \frac{T_0}{T} = 1 + \frac{\gamma-1}{2}\frac{u^2}{a^2} \tag{72}$$

At the stagnant cross section 0, the static temperature T_0 is equal to the total temperature T_{tot}; therefore,

$$\frac{T_{\text{tot}}}{T} = 1 + \frac{\gamma-1}{2}\text{M}^2,\ T\ = \frac{T_{\text{tot}}}{1+\frac{\gamma-1}{2}\text{M}^2}, \tag{73}$$

where M is the local Mach number. From Eqs. (64) and (73),

$$\frac{P_{\text{tot}}}{P} = \frac{T_{\text{tot}}^{\frac{\gamma}{\gamma-1}}}{T^{\frac{\gamma}{\gamma-1}}} = \left[\frac{T_{\text{tot}}}{T}\right]^{\frac{\gamma}{\gamma-1}} = \left[1 + \frac{\gamma-1}{2}\text{M}^2\right]^{\frac{\gamma}{\gamma-1}}, P = \frac{P_{\text{tot}}}{\left[1+\frac{\gamma-1}{2}\text{M}^2\right]^{\frac{\gamma}{\gamma-1}}} \tag{74}$$

4.4. Relationships of local Mach number, pressure and temperature of flows on adiabatic walls

Figure 5 shows the pressure distribution on a plane and an airfoil. On both the plane and the airfoil, boundary layers are formed. The pressure $P_{\text{local,bound}}$ in a boundary layer is almost equal to the pressure $P_{\text{local,main}}$ in a main flow outside of the boundary layer; therefore, the pressure in a boundary layer can be expressed by using relationships of the isentropic main flow. That is, $P_{\text{local,bound}} = P_{\text{local,main}}$. Afterwards, both the pressures are expressed as P_{local}.

The pressure distribution on a solid wall is usually expressed by pressure coefficient S_{local}, which is defined as:

$$S_{\text{local}} = \frac{P_{\text{tot,in}} - P_{\text{local}}}{\frac{1}{2}\rho u_{\text{in}}^2}, P_{\text{local}} = P_{\text{tot,in}} - \frac{1}{2}\rho u_{\text{in}}^2 S_{\text{local}} \tag{75}$$

but is sometimes expressed by another pressure coefficient η_{local}, which is defined as:

$$\eta_{\text{local}} = \frac{P_{\text{in}} - P_{\text{local}}}{\frac{1}{2}\rho u_{\text{in}}^2}, P_{\text{local}} = P_{\text{in}} - \frac{1}{2}\rho u_{\text{in}}^2 \eta_{\text{local}}. \tag{76}$$

The two expressions are related as follows:

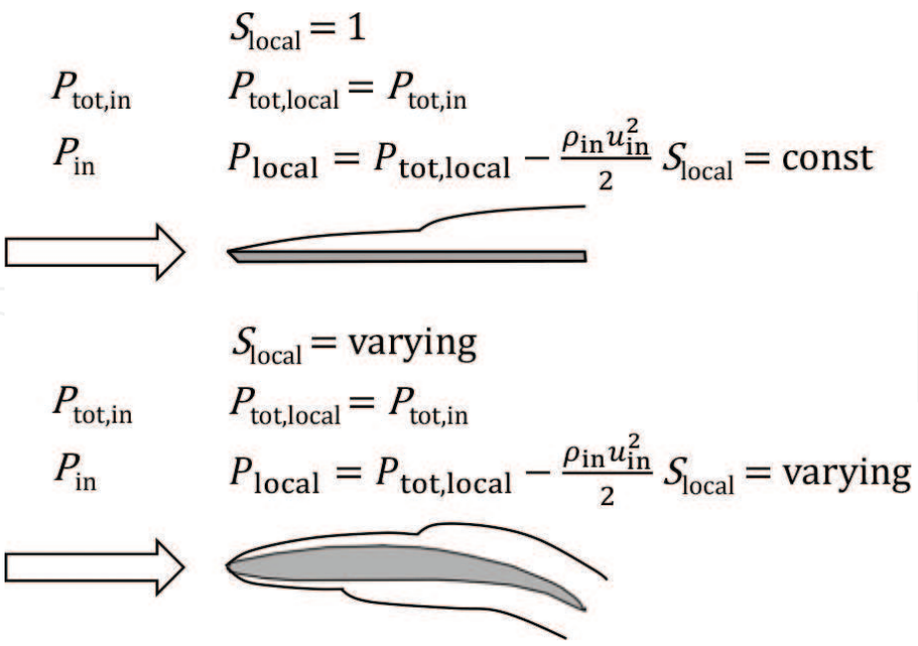

Figure 5. Pressure distributions of flows on a plane and an airfoil.

$$S_{local} = \frac{P_{tot,in} - P_{local}}{\frac{1}{2}\rho u_{in}^2} = \frac{P_{tot,in} - P_{in} + P_{in} - P_{local}}{\frac{1}{2}\rho u_{in}^2} = \frac{\frac{1}{2}\rho u_{in}^2 + P_{in} - P_{local}}{\frac{1}{2}\rho u_{in}^2} = 1 + \eta_{local}. \tag{77}$$

On a plane, S_{local} is unity everywhere; thus, P_{local} is constant everywhere. On the other hand, on an airfoil, S_{local} varies with the location; thus, P_{local} varies.

Figure 6 shows the temperature distribution on an adiabatic plane and an airfoil. In flows on an adiabatic wall, the total temperature $T_{tot,local}$ remains constant at the inlet total temperature $T_{tot,in}$. For incompressible flows, that is, with the Mach number $M_{local} = 0$, the static temperature T_{local} is always the same as $T_{tot,local}$. Then, T_{local} remains constant everywhere on both an adiabatic plane and an airfoil. On the other hand, for compressible flows, the Mach number M_{local} varies according to the following equation, which is derived from Eq. (74):

$$M_{local} = \sqrt{\frac{2}{\gamma - 1}\left\{\left[\frac{P_{tot,local}}{P_{local}}\right]^{\frac{\gamma-1}{\gamma}} - 1\right\}} \tag{78}$$

Here, the static temperature T_{local} varies with respect to M_{local} for compressible flows.

$$T_{local} = \frac{T_{tot,local}}{1 + \frac{\gamma-1}{2} M_{local}^2} \tag{79}$$

On an adiabatic plane, M_{local} is constant. Thus, T_{local} remains constant anywhere on an adiabatic plane, even in cases of compressible flows. On the other hand, on an adiabatic airfoil, M_{local} varies with the location; therefore, T_{local} varies in cases of compressible flows.

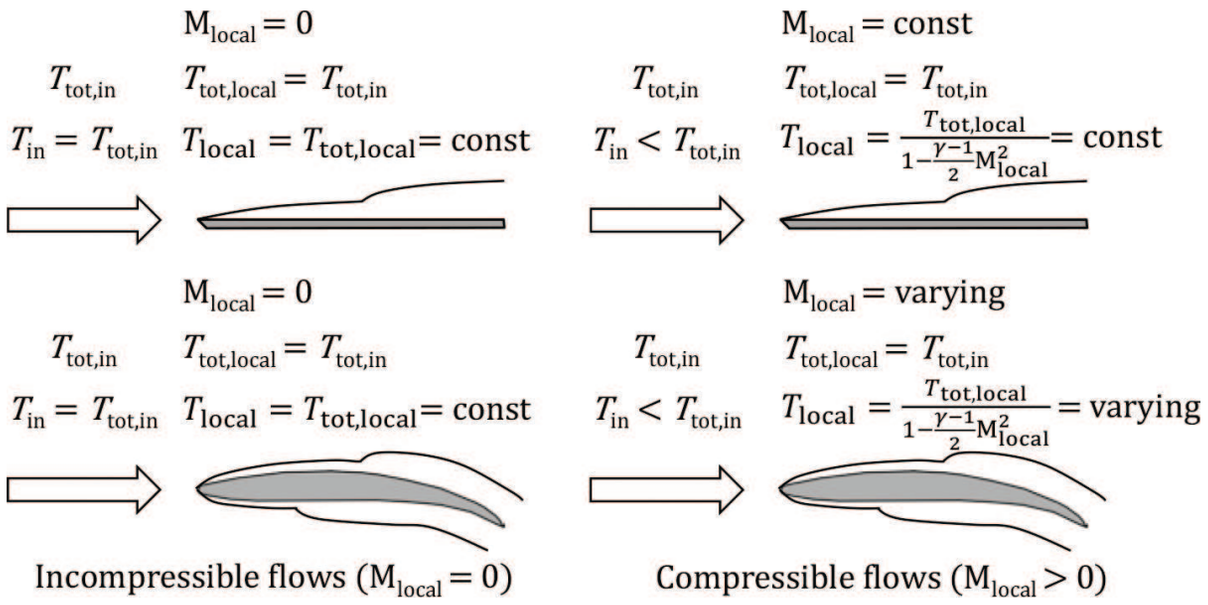

Figure 6. Temperature distributions of flows on an adiabatic plane and an airfoil.

4.5. Recovery temperature definition in boundary layer in compressible flow on adiabatic, heating and cooling walls

Eckert surveyed and organized the heat transfer in a boundary layer in a compressible flow on a wall [10]. In a boundary layer on an adiabatic plane, the adiabatic-wall temperature reaches T_r. This is called the "recovery temperature." **Figure 7** shows a schematic of the total temperature T_{tot} and static temperature T profiles, as well as the recovery temperature T_r in the vicinity of an adiabatic solid surface with a boundary layer in a compressible flow. As described in Section 4.1, a compressible flow has a measurable dynamic energy; then, the static temperature T in a boundary layer increases because of the braking effect, which converts a dynamic energy to a thermal energy. At the same time, heat generated by the braking effect conducts to the outside of the boundary layer. Therefore, the static temperature T and total temperature T_{tot} in the boundary layer approach the recovery temperature T_r on the wall, as shown in the middle in **Figure 7**.

In cases where a thermal boundary layer is completely inside a momentum boundary layer, that is, $Pr \geq 1$ the heat generated by the braking effect uses the rise of the static temperature T.. The recovery temperature T_r on an adiabatic wall is equal to the total temperature $T_{tot,main}$ of the main flow outside of the boundary layer. On the other hand, in cases where a thermal boundary layer protrudes from the edge of a momentum boundary layer, that is, $Pr < 1$, only part of the heat generated by the braking effect uses the rise of the static temperature T; then, the recovery temperature T_r on an adiabatic wall has an intermediate value between the total temperature $T_{tot,main}$ and the static temperature T_{main} of the main flow outside of the boundary layer. Eckert proposed an equation for the local recovery temperature $T_{r,local}$ on an adiabatic wall.

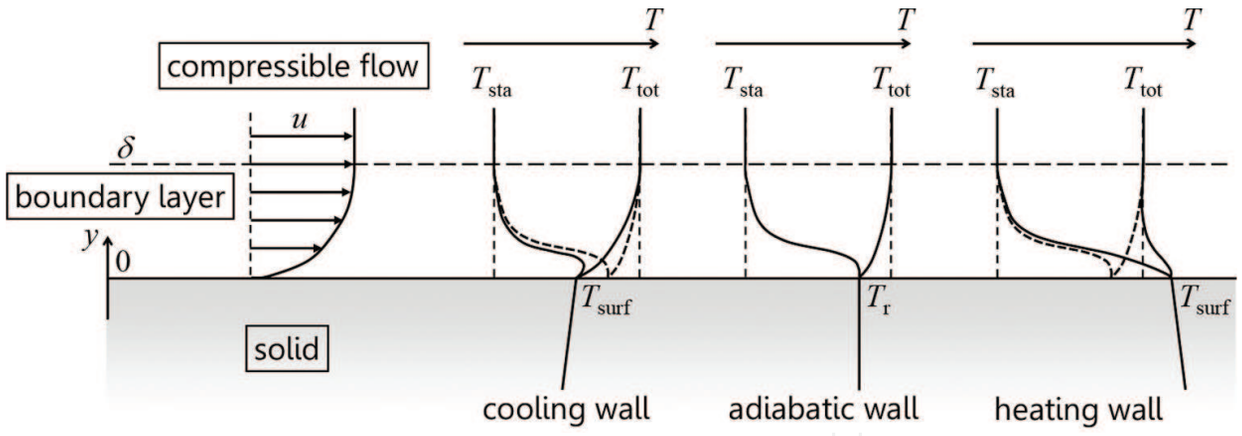

Figure 7. Total-, static-, and recovery-temperature profiles in the vicinity of cooling, adiabatic, and heating solid surfaces with a boundary layer in a compressible flow.

$$T_{\mathrm{r,local}} = T_{\mathrm{main}} + [T_{\mathrm{tot,main}} - T_{\mathrm{main}}] r_{\mathrm{local}} = T_{\mathrm{main}} + T_{\mathrm{dyn,main}} r_{\mathrm{local}} \tag{80}$$

$$r_{\mathrm{local}} = \begin{cases} \min(1, \mathrm{Pr}^{1/2}) & \text{for a laminar boundary layer} \\ \min(1, \mathrm{Pr}^{1/3}) & \text{for a turbulent boundary layer} \end{cases} \tag{81}$$

Here, r_{local} is the "temperature recovery factor," which is the ratio of the recovery temperature to the dynamic temperature of the main flow. Eckert mentioned that heat flux q_{local} in a boundary layer in a compressible flow should be defined as:

$$q_{\mathrm{local}} = h_{\mathrm{local}} [T_{\mathrm{r,local}} - T_{\mathrm{solid,local}}] \tag{82}$$

where h_{local} is the local heat transfer coefficient between a compressible flow and a solid wall. In the case where $q_{\mathrm{local}} = 0$, the local wall temperature $T_{\mathrm{solid,local}}$ equals the recovery temperature $T_{\mathrm{r,local}}$ and is called the "adiabatic wall temperature."

Here, Eckert's theory is extended to the recovery temperature T_{r} on a heating and cooling wall. In Eq. (80), the first term expressed by the static temperature T_{main} represents the internal energy that a local boundary layer originally has, and the second term expressed by the dynamic temperature $T_{\mathrm{dyn,main}} r_{\mathrm{local}}$ represents the net dynamic energy that is used to increase the temperature in a local boundary layer. When a local boundary layer is heated or cooled, the first term is affected, but the second term remains constant. The first term should be replaced by the appropriate form suitable for the heating or cooling of a boundary layer. Heating or cooling affects only a thermal boundary layer; therefore, the local total temperature $T_{\mathrm{tot,bound,x}}$ at the location x in the flow direction is defined as follows:

$$T_{\mathrm{tot,bound,x}} = T_{\mathrm{tot,in}} + \int_0^x \frac{q_{\mathrm{x}}}{\rho_{\mathrm{x}} C_{\mathrm{P}} \delta_{\mathrm{x}} u_{\mathrm{ave,x}}} dx \tag{83}$$

$$T_{\mathrm{bound,x}} = T_{\mathrm{tot,bound,x}} - T_{\mathrm{dyn,main,x}} \tag{84}$$

$$\rho_{\mathrm{x}} = \frac{P_{\mathrm{x}}}{R T_{\mathrm{bound,x}}} \tag{85}$$

$$\delta_{\mathrm{x}} = \begin{cases} 5\left[\frac{\nu}{u_{\mathrm{main,x}}\mathrm{Pr}}\right]^{0.5} x^{0.5} & \text{for a laminar boundary layer} \\ 0.37\left[\frac{\nu}{u_{\mathrm{main,x}}\mathrm{Pr}}\right]^{0.2} x^{0.8} & \text{for a turbulent boundary layer} \end{cases} \tag{86}$$

$$u_{\mathrm{x}} = \begin{cases} 0.5u_{\mathrm{main,x}} & \text{for a laminar boundary layer} \\ 0.8u_{\mathrm{main,x}} & \text{for a turbulent boundary layer} \end{cases}, \tag{87}$$

where $T_{\mathrm{bound,x}}$ and ρ_{x} are the static temperature and density, respectively, in a heated or cooled boundary layer, and δ_{x} and u_{x} are thermal boundary layer thickness and average velocity, respectively. Here, evaluations of δ_{x} and u_{x} are used for a plane, but more appropriate expression for a particular target flow field can be used. Finally, Eq. (80) is replaced by the following equation for the local recovery temperature of a heated or cooled boundary layer.

$$T_{\mathrm{r,local}} = T_{\mathrm{bound,x}} + T_{\mathrm{dyn,main,x}} r_{\mathrm{local}} = T_{\mathrm{tot,bound,x}} - T_{\mathrm{dyn,main,x}}[1 - r_{\mathrm{local}}] \tag{88}$$

5. Mach-number distribution on solid walls with various shapes

As described in Section 4 4, the local Mach number $\mathrm{M}_{\mathrm{local}}$ is constant on a plane but varies with the location on a single airfoil or an airfoil in a cascade. For a single airfoil, when the inlet Mach number M_{in}, the Reynolds number $\mathrm{Re}_{\mathrm{airfoil}}$ with a representative length of the airfoil chord L_{C}, and the angle of attack α are fixed, as

$$\mathrm{M}_{\mathrm{in}} = \frac{u_{\mathrm{in}}}{a_{\mathrm{in}}} \tag{89}$$

$$\mathrm{Re}_{\mathrm{airfoil}} = \frac{u_{\mathrm{in}} L_{\mathrm{C}}}{\nu_{\mathrm{in}}}, \tag{90}$$

the distribution of the local pressure coefficient S_{local} or η_{local} is uniquely obtained. In cases of a cascade of airfoils, when the stagger angle β and the solidity σ are fixed (see **Figure 8**), the distribution of the local pressure coefficient S_{local} or η_{local} is obtained. Fortunately, many

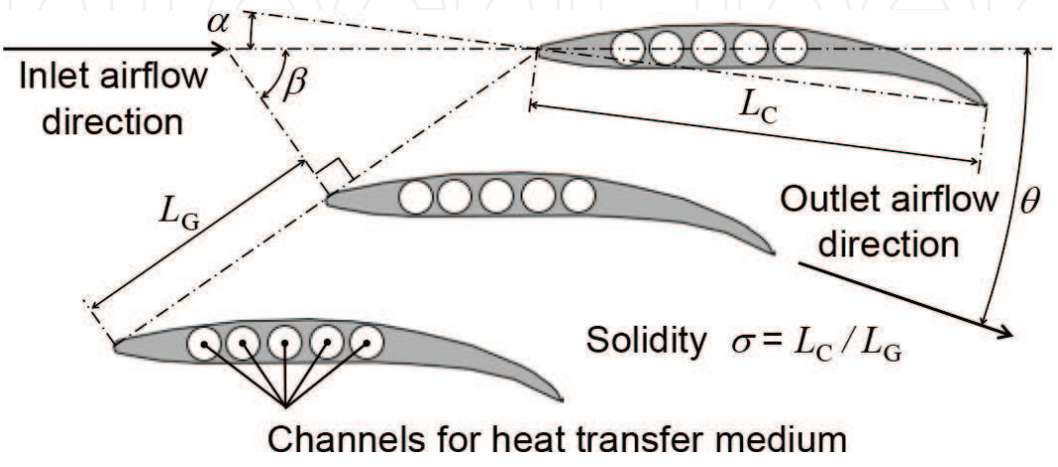

Figure 8. Flow field through a cascade of airfoils, where θ is the turning angle.

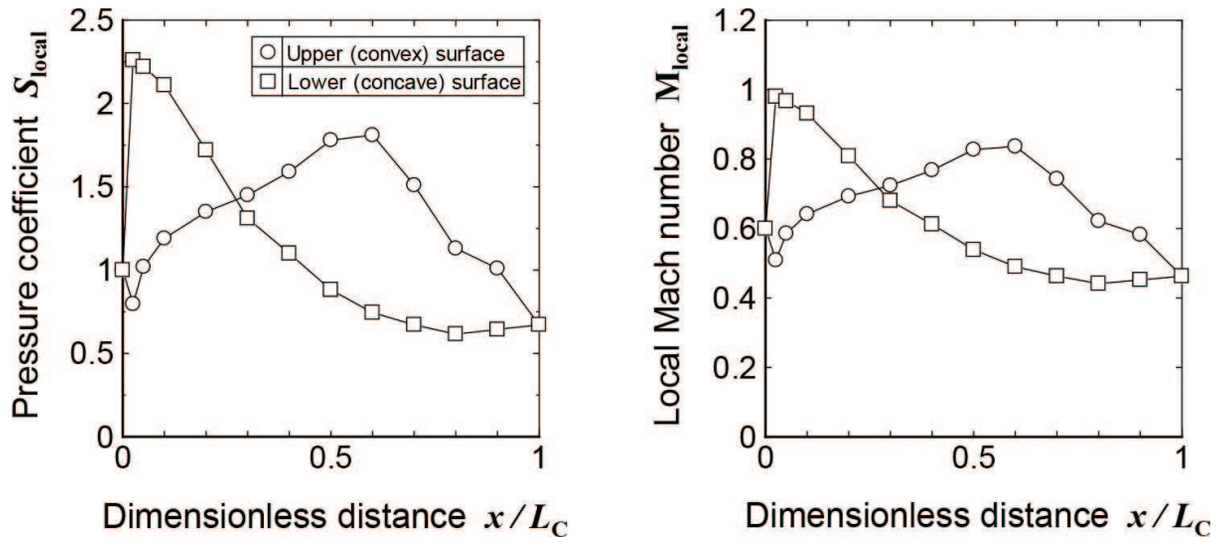

Figure 9. Local Mach-number distributions assumed from pressure-coefficient distribution.

experimental results of S_{local} or η_{local} have been reported for single airfoils and cascades of airfoils. The distributions of M_{local} are calculated using Eqs. (75), (76), and (78).

Ito et al. obtained distributions of M_{local} around an airfoil in a cascade of NACA65-(12$A_2$$I_{8b}$)10 airfoils, as shown in the right frame of **Figure 9**, from S_{local}, which is shown in the left frame of **Figure 9** [10].

6. Air-temperature distribution in boundary layers on solid walls

Nishiyama described in his book [11] that a developing boundary layer transforms from a laminar boundary layer to a turbulent boundary layer at $Re_x \cong 10^4$ in regions with adverse

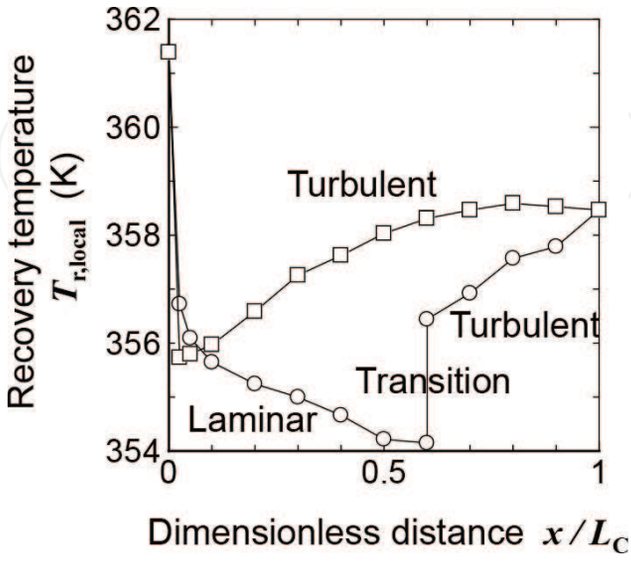

Figure 10. Recovery-temperature distribution assumed according to the pressure coefficient and local Mach number distributions in **Figure 9**.

pressure gradients, but a developing boundary layer transforms at $Re_x \cong 10^8$ in regions with favorable pressure gradients. This means that a developing boundary layer transforms across the minimum pressure point, that is, the maximum of the pressure coefficient S_{local} or η_{local} on the airfoil surface in cases of $Re_{airfoil} \cong 10^6$. According to the left graph of **Figure 9**, a developing boundary layer may transform at $x/L_C \cong 0.025$ on the lower concave surface and at $x/L_C \cong 0.6$ on the upper convex surface. Then, the local recovery temperature $T_{r,local}$ is assumed by using Eqs. (81) and (88) (see **Figure 10**). This $T_{r,local}$ can be used for the evaluation of the local heat flux q_{local} using Eq. (82) if an adequate heat-transfer coefficient h_{local} is employed.

7. Heat transfer through practical heat exchanger with complex shape

Ito et al. evaluated the rate of heat transfer from a hot compressible airflow to a cold supercritical-fluid flow through an airfoil heat exchanger, as shown in **Figure 8** [10]. Heat is transferred from the hot compressible airflow to the outer surface of the airfoil heat exchanger and is conducted from the outer surface to the five inner surfaces in the airfoil heat exchanger. Then, heat is transferred from the five inner surfaces of the airfoil heat exchanger to the cold supercritical-fluid flow inside the five tubes.

First, Ito et al. conducted wind-tunnel experiments. They installed n thermocouples into the airfoil heat exchanger and experimentally measured the temperature at n points inside the exchanger. Simultaneously, the air temperature and the air Mach number at the inlet, the supercritical-fluid temperature and pressure at the inlet, and the supercritical-fluid temperature at the outlet were experimentally measured.

Second, they assumed n heat-transfer coefficients $h_{air,1}$ to $h_{air,n}$ for the n parts of the air-contacted outer surface of the airfoil heat exchanger, as well as one heat-transfer coefficient h_{sfc} for the supercritical-fluid-contacted five inner surfaces of the airfoil heat exchanger.

Third, they performed an inverse heat-conduction analysis. The boundary conditions were set according to the experimental results for the distribution of the recovery temperature using the methods described in Sections 4.6, as well as the inlet supercritical-fluid temperature and pressure. Using these boundary conditions, heat-conduction calculations for the airfoil heat exchanger were conducted, and the temperatures at the n points in the airfoil heat exchanger and the outlet supercritical temperature were numerically obtained.

Finally, the $n+1$ numerically obtained temperatures were compared with $n+1$ experimentally obtained temperatures. If the temperatures were equal, the assumed $h_{air,1}$ to $h_{air,n}$ and h_{scf} were true. Otherwise, the assumed $h_{air,1}$ to $h_{air,n}$ and h_{scf} were corrected, and the inverse heat-conduction analysis was repeated.

Using these procedures, Ito et al. obtained an air Nusselt number correlation Nu_{air} for a cascade of NACA65-$(12A_2I_{8b})$10 airfoils, as shown in **Figure 8** [12].

$$Nu_{air} = 4.9410^{-3} Re_{airfoil} M_{in}^{1.44} \tag{91}$$

They also obtained a supercritical-fluid Nusselt number correlation Nu_{scf} for the tube flow given by Eq. (33).

Moreover, the heat-transfer rate Q_{entire} of an airfoil heat exchanger is estimated as follows:

$$Q_{entire} = \psi \kappa A_{scf} \Delta T_{lm,entire}, \tag{92}$$

where ψ is a correction factor for the airfoil heat exchanger, and ψ is the ratio of the actual heat-transfer rate to the heat-transfer rate of the ideal counter-flow heat exchanger without thermal resistance.

$$\psi = \frac{0.1236[0.02093|\xi| + 1]}{\phi_{scf} - \exp[-0.5\min\{1, \varepsilon_{SA}\}]} + 1 \tag{93}$$

Here, ξ is an incidence of air at the inlet. The incidence is a flow-direction angle from the airfoil camber (center) line at its leading edge, corresponding to an angle of attack of $\alpha = 9.47^{\circ}$ for the cascade in **Figure 8**. ϕ_{scf} and ϕ_{air} indicate the temperature effectiveness, as follows:

$$\phi_{scf} = \frac{T_{scf,out} - T_{scf,in}}{T_{air,in} - T_{scf,in}} \tag{94}$$

$$\phi_{air} = \frac{T_{air,in} - T_{air,out}}{T_{air,in} - T_{scf,in}} \tag{95}$$

Here, ϕ_{scf} and ϕ_{air} are positive for an air-cooled system and negative for an air-heated system. ε_{SA} is the ratio of the heat-capacity rates.

$$\varepsilon_{SA} = \frac{m_{scf} C_{P,scf}}{m_{air} C_{P,air}} \tag{96}$$

Here, m_{scf} and m_{air} are the mass flow rates of a supercritical-fluid and air, respectively, for an airfoil heat exchanger, and $C_{P,scf}$ and $C_{P,air}$ are the specific heats of a supercritical-fluid and air, respectively. κ is the overall heat-transfer coefficient for an ideal counter-flow heat exchanger without thermal resistance.

$$\kappa = \frac{1}{\frac{1}{h_{scf}} + \frac{1}{h_{air}} \frac{A_{scf}}{A_{air}}} \tag{97}$$

Here, A_{scf} and A_{air} are areas of supercritical-fluid-contact and air-contact surfaces, respectively, for an airfoil heat exchanger. $\Delta T_{lm,entire}$ is the logarithmic mean temperature difference:

$$\Delta T_{lm,entire} = \Phi[T_{air,in} - T_{scf,in}] \tag{98}$$

Φ is the ratio of the logarithmic mean temperature difference to the temperature difference between the inlet air temperature and the supercritical-fluid temperature.

$$\Phi = \begin{cases} 1 & \text{for} \varepsilon_{SA} = 1 \\ \dfrac{|\phi_{scf}| - |\phi_{air}|}{\ln\left[\dfrac{\phi_{air}}{\phi_{scf}}\right]} & \text{for} \varepsilon_{SA} \neq 1 \end{cases} \tag{99}$$

The actual heat-exchange rate is estimated as Q_{entire}[numberofairfoils].

For example, Ito et al. performed cycle calculations for an intercooled and recuperated jet engine employing several pairs of airfoil heat exchangers whose heat-transfer performance is evaluated by Eqs. (91)–(99) [13].

These examples can be used for a cascade of airfoil heat exchangers; therefore, the air Nusselt number correlation in Eq. (91) or thermal resistance in Eq. (93) might be further modified in the near future according to the progress of research, as knowledge in this field is still developing.

8. Conclusion

The Nusselt number between supercritical fluid flows and solid walls can be estimated by appropriate conventional correlations using the Reynolds and Prandtl numbers if sufficiently accurate physical properties are used for each local point through the region of supercritical fluid flows. Thus, a numerical integration of local heat flow rate is required when you calculate the entire heat flow rate in a heat exchanger between supercritical fluid flows and solid walls.

The recovery temperature should be considered for the estimation of heat transfer between compressible flows and solid walls. For compressible flows on adiabatic airfoil surfaces, the local recovery temperature varies by each point on the airfoil surface, owing to the accelerating and decelerating effects of the main flow outside of the boundary layer on the airfoil surface. In addition, for compressible flows on cooling and heating airfoil surfaces, the local total temperature on airfoil surfaces in the boundary layer also varies at each point because of cooling and heating effects. The accelerating and decelerating effects can be estimated from the local Mach number distribution on the airfoil shape. The cooling and heating effects can also be estimated when a numerical integration of elapsed variation of the local total temperature along the boundary layer from the leading edge if the detailed solid temperature distribution on the airfoil surface is known. To obtain the detailed solid temperature distribution on the airfoil surface, detailed experimental measurements or an accurate CFD analysis may be required.

To estimate conjugate heat transfer through a practical heat exchanger with a complex shape, one solution is a combination of experimental results in wind tunnel tests and an inverse heat conduction method. The other solution is CFD analysis validated by experimental results in wind tunnel tests. Empirical correlations are very limited for conjugate heat transfer through a practical heat exchanger with complex shape because knowledge in this field is still developing.

Author details

Yu Ito

Address all correspondence to: itoyu110@00.alumni.u-tokyo.ac.jp

Tokyo Institute of Technology, Yokohama, Japan

References

[1] Stanley HE. Introduction to Phase Transitions and Critical Phenomena. Oxford, UK University Press; 1971.

[2] Span R, Wagner W. A New Equation of State for Carbon Dioxide Covering the Fluid Region from the Triple-Point Temperature to 1100 K at Pressures up to 800 MPa. Journal of Physical and Chemical Reference Data. 1996;**25**.

[3] Vesovic V, Wakeham WA, Olchowy GA, Sengers JV, Watson JTR, Millat J. The Transport Properties of Carbon Dioxide. Journal of Physical and Chemical Reference Data. 1990;**19**.

[4] Wagner W, Pruß A. The IAPWS Formulation 1995 for the Thermodynamic Properties of Ordinary Water Substance for General and Scientific Use. Journal of Physical and Chemical Reference Data 2002;**31**.

[5] Huber ML, Perkins RA, Laesecke A, Friend DG, Sengers JV, Assael MJ, Metaxa IN, Vogel E, Mareš R, Miyagawa K. New International Formulation for the Viscosity of H_2O. Journal of Physical and Chemical Reference Data 2009;**38**.

[6] Huber ML, Perkins RA, Friend DG, Sengers JV, Assael MJ, Metaxa IN, Miyagawa K, Hellmann R, Vogel E. New International Formulation for the Thermal Conductivity of H_2O. Journal of Physical and Chemical Reference Data . 2012;**41**.

[7] Dittus FW, Boelter LMK. Heat Transfer in Automobile Radiators of the Tubular Type. The University of California Publications in Engineering. 1930;**2**.

[8] Liao SM, Zhao TS: Measurements of Heat Transfer Coefficients from Supercritical Carbon Dioxide Flowing in Horizontal Mini/Micro Channels. Journal of Heat Transfer. 2002;**124**.

[9] Ito Y, Inokura N, Nagasaki T. Conjugate Heat Transfer in Air-to-Refrigerant Airfoil Heat Exchangers. Journal of Heat Transfer. 2014;**136**.

[10] Eckert ERG. Survey of boundary Layer Heat Transfer at High Velocities and High Temperature. Wright Air Development Center (WADC) TR 59–624, 1960.

[11] Nishiyama T, Yokugata Nagare Gaku [translated as "Aerodynamics of Airfoil"]. p. 23, *Nikkan Kogyo Shimbun Ltd.* (*Business & Technology Daily News*), Tokyo, 1998, in Japanese.

[12] Ito Y, Goto T, Nagasaki T. Effect of Airflow on Heat Transfer of Air-to-Refrigerant Airfoil Heat Exchanger. AIAA-2015-1193, 2015.

[13] Ito Y, Inokura N, Nagasaki T. Intercooled and Recuperated Jet Engine Using Airfoil Heat Exchangers. ISABE2015-20100, 2015.

IntechOpen

IntechOpen